AIAA JOURNAL
Vol. 31, No. 8, August 1993

Instantaneous Topology of the Unsteady Leading-Edge Vortex at High Angle of Attack

C. Magness,* O. Robinson,* and D. Rockwell†
Lehigh University, Bethlehem, Pennsylvania 18015

A new topological structure is defined for flow over a delta wing undergoing transient pitching maneuvers at high angle of attack. This instantaneous structure differs substantially from the traditional topology observed for stationary wings at low angle of attack. The leading edge vortex is found to exhibit an outward-spiraling motion corresponding to an unstable focus. In addition, the streamlines separating from the leading edge are not entrained into the vortex core in the instantaneous sense. The instantaneous topology is determined from high-resolution measurements over the crossflow plane by locating and categorizing the critical points of the instantaneous sectional streamlines. The three-dimensional, instantaneous streamline pattern corresponding to this topological structure is constructed by phase referencing the velocity fields at various chordwise locations. This approach allows three-dimensional characterization of the unstable focus of the leading-edge vortex and its relation to the feeding sheet.

Nomenclature

Å	=nondimensional pitch rate, $\dot{\alpha}C/2U_\infty$
C	=root chord length
N_i	=node critical point
N_i'	=half-node critical point
S_i	=saddle critical point
S_i'	=half-saddle critical point
s	=local semispan of wing, $x \tan \gamma$
U_∞	=freestream velocity
x,y,z	=wing-fixed coordinate system (origin at apex)
α	=angle of attack
α_f	=final angle of attack of pitching maneuver
α_i	=initial angle of attack of pitching maneuver
$\dot{\alpha}$	=circular pitch rate
γ	=semiapex angle
Λ	=sweep angle
ξ,η,ζ	=nondimensional wing-fixed coordinate system (origin at apex); $\xi=x/C$, $\eta=y/s$, $\zeta=z/s$

Subscript

i	=critical point index

I. Introduction

INTEREST in supermaneuverability has stimulated research into unsteady flows past delta wings. These unsteady flows are typified by large angular excursions in angle of attack (or roll or yaw) occurring over relatively short time scales.[1] Several recent investigations have studied the effects of pitching maneuvers at high angles of attack. Flow visualization studies such as those of Reynolds and Abtahi,[2] Magness et al.,[3] and Jarrah[4] have provided information on the response of the vortex breakdown phenomenon during transient maneuvers. Atta and Rockwell[5] and LeMay et al.[6] describe the response for harmonic pitching of the delta wing. Woffelt[7] addresses both of these types of pitching motions. These and other studies have observed the hysteresis of the location of vortex breakdown during unsteady motion of the wing relative to quasisteady locations. Quantitative force and moment measurements conducted by Woffelt,[7] Soltani et al.,[8] Jarrah,[4] and Ashley et al.,[9] among others, have shown similar hysteresis in the quantitative parameters. In a preliminary report on the present work, Magness et al.[10] noted a similar hysteresis, or lag, in vortex breakdown response in the pattern of the crossflow velocity field. A comprehensive summary of recent experiments is given by Ashley et al.[9]

The foregoing research has provided useful quantitative information and valuable flow visualization. The fluid dynamics of the flow, however, have not been addressed in detail; flow visualization by smoke or dye injection cannot provide, for example, instantaneous streamline patterns in the crossflow plane. To date, the unsteady flow structure during transient pitching maneuvers has remained unidentified; however, the experiments noted earlier suggest that it differs from the corresponding quasisteady flow structure.

Topological concepts can effectively characterize flow structure by simply defining essential features and their interrelationships. Two flows may be said to be structurally equivalent if they are topologically equivalent.[11] Critical points are the features used for topological identification; in a velocity field, they are the locations at which the slope of the streamline becomes indeterminate. Streamline trajectories connecting the various critical points provide the fingerprint of the given flow. A classification of critical points and the concept of topological equivalence are described by Hunt et al.[12] Hornung and Perry[13] have examined bifurcation lines and stream surfaces in regard to three-dimensional separation for both slip and no-slip critical points. A general mathematical development describing the allowable critical point combinations in three-dimensional flows is given by Chong et al.[14]

Complex flows over a stationary delta wing have been described in detail using topological descriptions with particular emphasis on the visualized surface flow patterns. Tobak and Peake[15] provide a useful review of the concepts and benefits of such a description. With regard to the topology of the flow above the wing, Carcaillet et al.[16] and Su et al.[17] present patterns corresponding to steady flow past stationary wings at low angle of attack. In their topological representations, the leading-edge vortex appears as a stable, inward-spiraling focus. In fact, this representation is the traditional view of the leading-edge vortex.

The goal of the present investigation is to characterize, for the first time, the instantaneous topology of the crossflow over a delta wing in maneuver, as initially reported by Magness et al.[18] Using particle image velocimetry, high-resolution two-dimensional velocity fields will be produced; they will lead to definition of the critical-point flow patterns. Of particular interest are the features of the topological structure during the maneuver relative to the

Received Aug. 9, 1991; revision received July 27, 1992; accepted for publication Aug. 12, 1992.

*Postdoctoral Fellow, Department of Mechanical Engineering.
†Paul B. Reinhold Professor, Department of Mechanical Engineering. Member AIAA.

case of the stationary wing and the degree to which the structure of the transient flowfield is stable. Moreover, the instantaneous three-dimensional flow structure will be pursued by considering a number of chordwise locations along the wing and employing a newly developed image construction technique.

II. Experimental Techniques

The experiments were carried out in an open surface water channel. The test section height and width had dimensions of 610 and 914 mm; its length was 4.6 m.

The Plexiglas delta wing was mounted within this test section; its geometry is illustrated in Fig. 1. The sweep angle Λ is 75 deg. The lee side is flat, and the leading edges are beveled at 40 deg on the windward side. The root chord $C = 242$ mm. The freestream velocity $U_\infty = 38$ mm/s provides a chord Reynolds number of 9.2×10^3. This Reynolds number is sufficiently low to provide a laminar flowfield in the absence of vortex breakdown. For the current experiments, a ramp-type pitching maneuver is employed that consists of constant pitching rate between initial α_i and final α_f angles of attack; both pitch-up and pitch-down motions are employed. Values of the nondimensional pitch rate Å are varied in the range from 0.25–0.15. The extreme values of angle of attack are 25 and 50 deg. For the stationary wing, at $\alpha = 25$ deg, vortex breakdown occurs downstream of the trailing edge of the wing. At $\alpha = 50$ deg, the stationary breakdown location is approximately at $\xi = 0.15$, where $\xi = x/C$ with $x = 0$ defined at the apex.

Particle Image Photography

Particle image velocimetry (PIV) is a diagnostic technique capable of providing the instantaneous velocity field over an entire plane of the flow. A historical development of the technique is given by Dudderar et al.,[19] and a technical assessment is given by Adrian.[20] In this technique, the flowfield is seeded with particles on the order of 10 μm in diameter. As the particles are displaced within a pulsating sheet of laser light, they are multiply exposed; the resultant image is captured on a single negative. Typically, the multiple exposures may be created by chopping a continuous wavelength laser or doubly pulsing a pulsed laser. Each negative then contains a large number of particle pairs with the displacement being proportional to the local velocity. The negative may be automatically interrogated using image processing hardware and computer software by one of several procedures as explained by Adrian.[20] The result is typically a high-resolution two-dimensional array of velocity vectors representing the original flow.

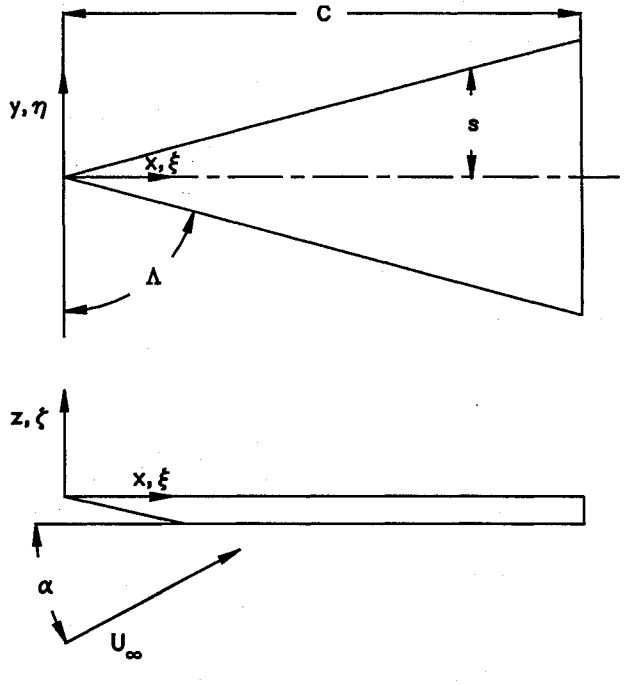

Fig. 1 Overview of the delta wing.

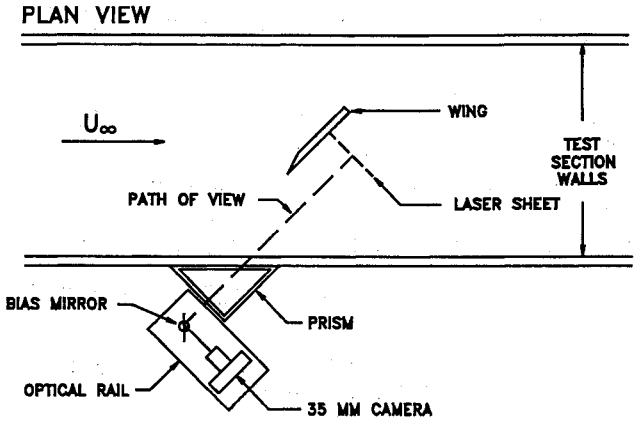

Fig. 2 Overview of photographic configuration.

The present particle imaging system uses an Argon-ion laser operating in the multiline mode providing essentially 4 W of continuous power. In place of the traditional beam-chopping device, a laser scanning technique is employed to provide a higher effective intensity of illumination. The experimental technique is briefly described in the following; for a more detailed discussion of the laser scanning technique the reader is directed to Magness et al.[21] or Magness.[22] A 2-mm laser beam is steered via mirrors through a focusing lens system to an oscillating mirror driven by a General Scanning G120D galvanometer scanner; it scans the beam across the flowfield to generate a fanlike sheet of light. The beam diameter determines the sheet thickness; within the test section it is approximately 2 mm. The scanner is driven with the output from a ramp function generator, thereby providing a uniform scan in one direction across the flow, followed by a rapid return to the starting position for the next scan. The scanning rate is variable; in the present experiment, a scan frequency of 100 Hz was found to be optimal.

The fanned sheet of laser light is oriented to illuminate the crossflow plane of the delta wing by rotating the sheet to intersect the wing normally (Fig. 2). The flow is seeded with 4-μm (TSI model 10087) metallic-coated particles that provide high reflectivity. For this experiment, the sheet of laser light is adjusted to be normal to the lee surface of the wing at the angle of attack at which the photographs are taken. In the present study, this instantaneous angle of attack is 45 deg.

The line of sight through the camera is perpendicular to the laser sheet to focus over the entire field of view. This requires a viewing angle of 45 deg relative to the wall of the test section. Refraction effects are significant at such large viewing angles. Consequently, it was necessary to design and implement a Plexiglas water-filled prism to compensate for and eliminate refraction effects. The prism is affixed to the exterior wall of the test section (see Fig. 2). The light rays passing through the prism first refract in one direction at the water-Plexiglas interface inside the water channel, then refract back in the other direction at the Plexiglas-water interface inside the prism. Since the two interfaces involve equivalent media, the overall effect is to translate the resulting rays slightly without a significant change in angle of propagation. Thereafter, the light rays pass out of the prism normal to the prism wall. The absence of refraction effects was ascertained by photographing a fine rectangular grid collinear with the laser sheet.

The image from the flowfield passes through the prism, is reflected from a bias mirror, and is then transmitted to the lens of the Nikon F4 35-mm camera. The photographic issues are addressed by Lourenco and Krothapalli.[23] The bias mirror is inserted into the optical path of the camera at 45 deg, thus making the camera axis perpendicular to the viewing axis (see Fig. 2). A General Scanning G325D galvanometer scanner rotates the bias mirror. This bias mirror offsets the reverse flow velocities so that their direction and magnitude can be determined unambiguously. After all flow velocities have been calculated, the bias is removed and the actual velocities are obtained. This technique was origi-

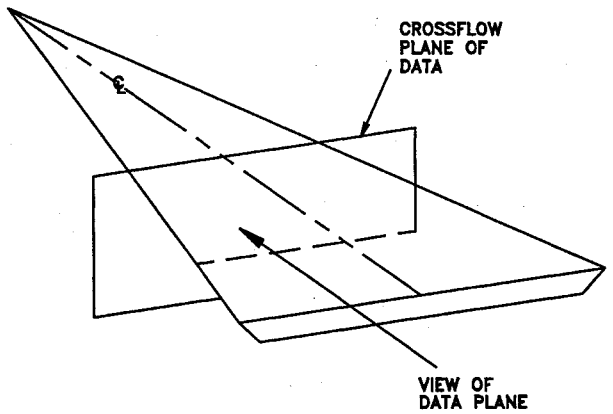

Fig. 3 Definition of view of crossflow velocity field over the delta wing.

nally advanced by Adrian,[24] who also provides a more in-depth explanation of the concept.

Control of the experiment is performed by a central microcomputer, which synchronizes the forced motion of the wing in conjunction with the laser scanning, bias mirror rotation, and camera firing. The camera is fired when the instantaneous angle of attack reaches 45 deg during the pitch-up or pitch-down maneuver. The laser scanning parameters are adjusted so that typically four images of each particle are exposed during one shutter opening. This is accomplished by a high rate of scanning relative to the shutter speed.

Image Interrogation

The velocity information is generated from the negative of the photograph by an automatic interrogation system having an optical arrangement similar to that of Meynart[25]; the automatic control of the interrogation is derived from that of Lourenco and Krothapalli.[26] The negative is placed into a stepper-motorized x-y traverse that is controlled by a software overseeing the interrogation process. A Helium-Neon laser beam passes through the negative, through an objective lens, and then to a video camera where the resulting image is digitized for automatic processing.

This technique produces Young's fringes in the far field of the negative. These fringes represent the overlapping diffraction patterns from the particle images; they are an optical Fourier transform of the original negative. The fringes are oriented normal to the direction of motion, and the fringe frequency is directly proportional to the particle displacement and, hence, to the local velocity vector. By digitizing Young's fringe pattern and then analyzing the digitized pattern with an autocorrelation technique, it is possible to obtain the velocity vector at a given location on the negative. The entire negative is interrogated in this manner. The result is a fine grid of velocity vectors corresponding to a two-dimensional velocity field. This technique is assessed and discussed in detail by Lourenco et al.[27] and Adrian.[20]

In the current experiments, the photographs are taken at a magnification factor of 0.25. Upon interrogation, the grid size is typically 80 × 80, producing 6400 velocity vectors. The negative is interrogated with a 0.25-mm spacing in both the x and y directions, which yields a real flow spacing of 1 mm. The interrogation beam diameter is 0.591 mm, however, so that the interrogation points overlap each other. In this way, a smooth transition between adjacent velocity vectors is incorporated into the data acquisition. Furthermore, in regions where data density may be low, this overlapping allows for the acquisition of a more continuous field.

Particle Image Postprocessing

The raw, unprocessed vector fields generated by the interrogation process contain spurious data due to factors such as locally low particle density. "Holes" or data dropout are present in the data for similar reasons. Data dropout in the separating shear layer from the leading edge is due to the large velocity gradient in that region. Closely spaced particle images representing large differences in velocity magnitude within the domain of the interrogation beam cause noise in the fringe pattern because no one dominant velocity is present. As a result, neither velocity is detected. Because of these considerations, it is not possible to resolve the detailed structure of the separating shear layer with the field of view currently employed.

The first step in postprocessing consists of removing the obviously "bad" vectors. This can be done either manually or automatically. Automatic rejection may be used; it judges a vector against its neighbors and selectively removes vectors that fail to meet certain criteria for length ratio and angular deviation. Typical criteria that yield good results are a 30% variation in magnitude and 30-deg variation in direction. Examples of both the raw vector field and the resultant data after rejection are shown in Magness.[22]

To analyze physical details of the flowfield, the regions of data dropout must be interpolated appropriately. The bilinear method described by Landreth and Adrian[28] is used herein to generate the interpolated field in each case. The interpolation method employed is acceptable so long as the size of the dropout region is small relative to the length scales of interest in a given portion of the flow. Furthermore, as each interrogation spot overlaps its neighbor, dropouts with widths of one grid spacing should be adequately interpolated. For the present case, the grid resolution is on the order of 1 mm. The shear-layer thickness is at least one order of magnitude smaller than this and beyond the scope of the current arrangement. Therefore, interpolation in that region is of less importance than the limits of the resolution. The vortex core, however, is on the order of 10 mm so that the present resolution is quite sufficient. The secondary vortices are not of immediate concern but are on the order of the resolvable scales.

III. Experimental Results

Instantaneous Crossflow Velocity Field

A typical plane for the PIV measurements made herein is defined in Fig. 3; each plane is normal to the wing lee surface. The port half of the wing is visualized to increase the spatial resolution. The flow patterns occurring on the unvisualized starboard side of the wing are qualitatively equivalent to those on the port side, and in certain instances their structure and topology can be extrapolated from those on the port side.

An interpolated velocity field typical of the fields generated for the present work is shown in Fig. 4; these data correspond to a chord location $\xi = 0.79$ and an angle of attack $\alpha = 45$ deg during a pitch-up maneuver from $\alpha_i = 25$ deg to $\alpha_f = 50$ deg at a pitch rate of $\dot{A} = 0.15$. The image employed to interrogate this data is generated using image shifting so that the reversed velocities can be determined unambiguously. In Fig. 5, the corresponding unshifted particle images are shown; these images correspond to a signifi-

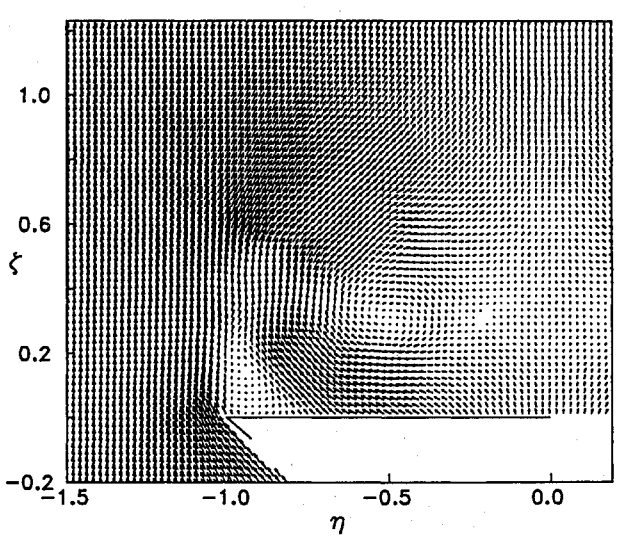

Fig. 4 Instantaneous velocity field resulting from interpolation. The data are taken at $\xi = 0.79$ and $\alpha = 45$ deg during a pitch-up maneuver from $\alpha_i = 25$ deg to $\alpha_f = 50$ deg with pitch-rate $\dot{A} = 0.15$.

cantly lower particle density than that employed during the image-shifting experiments. Therein, the particle displacements near mid-span are indistinguishable; however, with the addition of sufficient image shifting they are readily interrogated. Figure 5 represents the method of flow visualization most suitable for comparison with the data acquired by the PIV method; the time-exposed tracks of the particles correspond directly to the measured velocities and provide a qualitative description of the instantaneous flowfield. Comparable visualization is not possible with conventional methods such as hydrogen bubble or dye injection. These methods cannot provide instantaneous descriptions of the entire crossflow plane and typically carry some history of the flow. The general flow structure observed in Figs. 4 and 5 is characteristic of the flow structure noted at α = 45 deg during pitch-up motions with

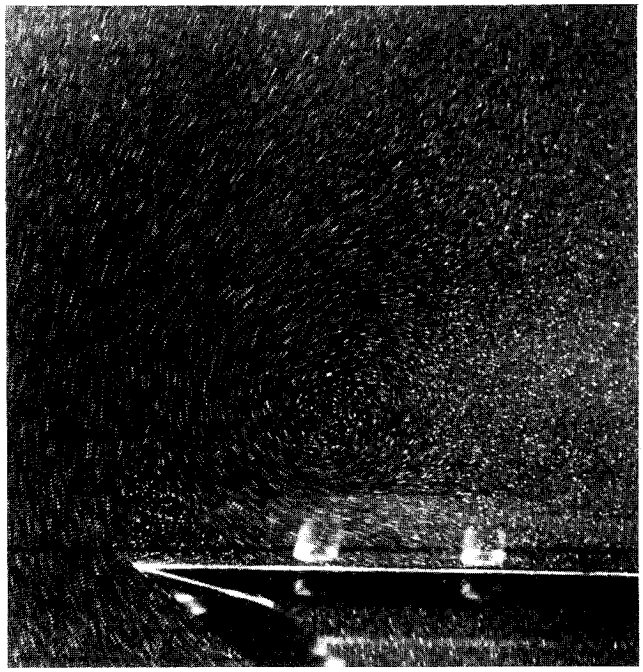

Fig. 5 Unshifted particle image corresponding to conditions in Fig. 4: ξ = 0.79 and α = 45 deg during a pitch-up maneuver from α_i = 25 deg to α_f = 50 deg with pitch rate $\dot{A}$ = 0.15. Density of images is much less than that employed during acquisition of quantitative, image-shifted data.

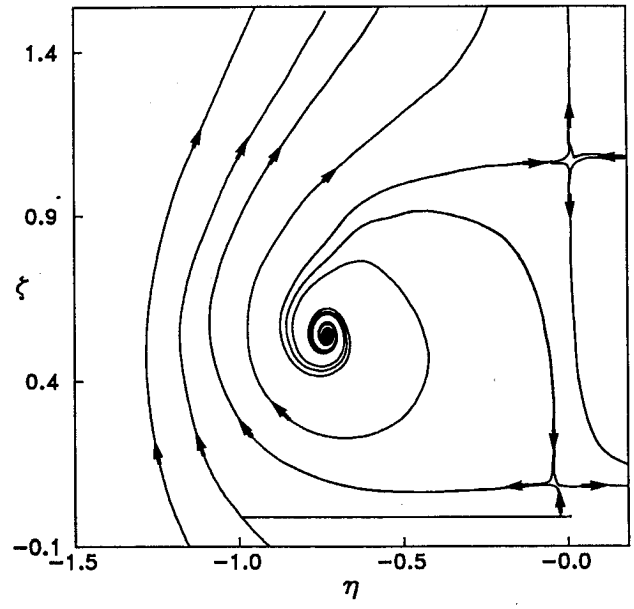

Fig. 6 Instantaneous sectional streamlines calculated from velocity field corresponding to ξ = 0.79 and α = 45 deg during pitch-up motion from α_i = 25 deg to α_f = 50 deg with pitch rate $\dot{A}$ = 0.05.

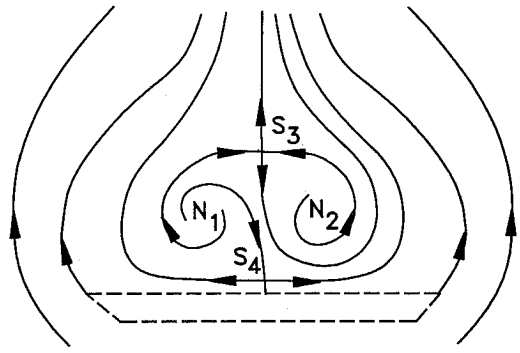

Fig. 7 Definition of topology of instantaneous streamline pattern at ξ = 0.79 and α = 45 deg during pitch-up motion from α_i = 25 deg to α_f = 50 deg with pitch rate $\dot{A}$ = 0.05. Pattern corresponds to laboratory reference frame.

the same initial and final angles of attack over a wide range of pitching rates from $\dot{A}$ = 0.025 to 0.15. This crossflow pattern is also found over a major portion of the wing, as discussed in the following section.

Instantaneous Topological Structure

The flow structure in desired planes of the flow can be defined by sectional streamlines. These special streamlines are neither true instantaneous streamlines nor projections of them. They are simply the integrated two-dimensional velocity data over a given plane. The planar structure revealed by these sectional streamlines, however, is of central importance in understanding the global three-dimensional flow structure.[29]

Sectional streamlines were calculated for the instantaneous crossflow velocity field at the chord location ξ = 0.79 and corresponding to an instantaneous angle of attack α = 45 deg and pitch rate $\dot{A}$ = 0.05 for a pitch-up maneuver from α_i = 25 deg to α_f = 50 deg; these streamlines are plotted in Fig. 6. The streamline pattern portrays the various interconnections between the focus (vortex center), saddle points, and paths of the separated flow around the leading edge. Furthermore, the separatrices, or streamlines emanating from the (half-) saddle points, define the regions of the flow that are separate from one another. Figure 7 shows the representative topology inferred from Fig. 6. This schematic also includes the topology of the starboard side of the wing, inferred from the data on the port side. It is important to note that the central features of Fig. 7—the outward-spiraling vortex core and the lack of flow entrainment from the freestream—are discernible in the flow visualization of Fig. 5. In Fig. 7, the reference frame corresponds to the laboratory frame and the wing is shown in phantom to indicate that it is nonstationary with respect to the reference frame. Because of the motion of the wing, there are no critical points on the wing surface. A saddle point S_4 is also present due to this choice of reference frame.

Figure 7, although derived from Fig. 6 at a pitch rate of $\dot{A}$ = 00.5, is representative of the cross-sectional topology in the laboratory reference frame for pitch rates in the range $\dot{A}$ =0.025–0.15 with all other pitching parameters identical. This fact is due to the similarity of the crossflow velocity fields for these conditions as mentioned in the preceding section.

Application of a velocity shift in the negative y direction leads to a change of reference frame that can account for various effects due to the motion of the wing and the motion of the vortex field with respect to the wing. A velocity shift proportional to the pitch rate is added to the velocity fields corresponding to the conditions of Fig. 6 and pitch rates in the range of $\dot{A}$ = 0.025–0.15; this computation produces the velocity fields in moving reference frames. Figure 8 illustrates the effect of this modification on the streamline patterns at α = 45 deg for a pitch-up motion (from α_i = 25 deg to α_f = 50 deg at ξ = 0.79) for the cases of $\dot{A}$ = 0.05 and 0.10, respectively. The topology corresponding to this streamline pattern is defined in Fig. 9; it represents the topology in the moving reference frame. The advantage of this moving reference frame is that it allows for more

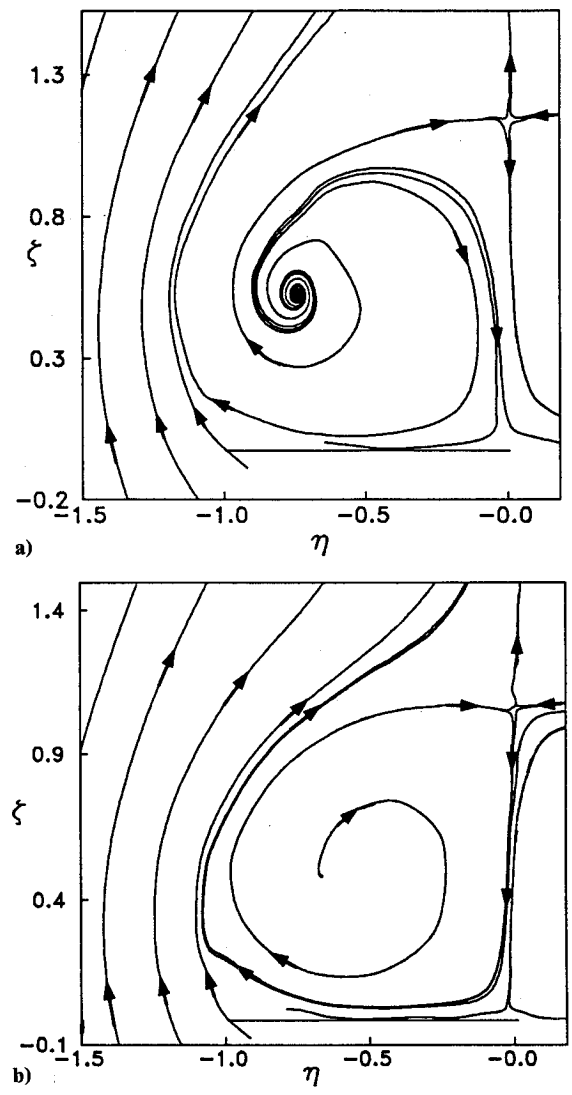

Fig. 8 Instantaneous sectional streamlines calculated from velocity field corresponding to $\xi = 0.79$ and $\alpha = 45$ deg during pitch-up maneuvers from $\alpha_i = 25$ deg to $\alpha_f = 50$ deg. The respective pitch rates are a) $\hat{A} = 0.05$ and b) $\hat{A} = 0.10$.

direct comparison with stationary wing topologies. The saddle point denoted as S_4 in Fig. 7 is not present in Fig. 9; it has been shifted vertically downward into the wing and appears as a half-saddle point of attachment S_4' in Fig. 9. Two additional half-saddle points of separation, S_1' and S_2', are now indicated at the leading edges because the wing is no longer moving with respect to the reference frame. With the exception of these three half-saddle points, the remainder of the topological pattern is qualitatively equivalent to that corresponding to the laboratory reference frame (Fig. 7).

A notable feature of Figs. 7 and 9 is the pathway of flow, or alleyway, between the separatrix flowing out and downward from saddle point S_3 and the separatrix flowing downward into saddle point S_4 (or S_4'); this alleyway signifies the instantaneous flow of fluid from one side of the wing to the other. The presence of this alleyway indicates that the port and starboard vortex fields are asymmetrical; they are not, in the instantaneous sense, separated by a symmetry condition. Careful examination of Figs. 8a and 8b shows that the direction of flow in this alleyway is to the right in Fig. 8a and to the left in Fig. 8b. The lack of a direct connection of saddle point S_3 to S_4 (or S_4') in Figs. 7 and 9 is not a surprising result. Perry and Chong[29] point out that saddle-to-saddle connections are structurally unstable and may only exist instantaneously during a bifurcation event; i.e., during a change of topological structure. In this case, the change in direction of flow in the alleyway is a bifurcation. The inherent unsteadiness and asymmetry of the vortex breakdown location observed in the present flow appears to indicate that the direction of flow in the alleyway continuously alternates from side to side as a consequence of this asymmetry. This awkward topological feature serves to underscore the basic asymmetry present in a geometrically symmetric flow; such asymmetry has been noted previously on low-aspect ratio stationary wings.[30] Therefore, Figs. 7 and 9 illustrate the representative topology since they include the presence of the alleyway. It is implicitly assumed that the direction of the alleyway varies and that its instantaneous direction does not play a large role in determining the flow structure.

For comparison, Fig. 10 shows the topology for the case of a stationary delta wing at an angle of attack $\alpha = 20$ deg based on the previous experimental work of Magness et al.[3] All critical points are inferred from these data in conjunction with the data of Carcaillet et al.[16] and Su et al.,[17] which also correspond to a stationary delta wing at low angle of attack. The presence of S_2 and S_5' are necessary both for completeness of the topology and for fulfillment of the topological rule for a two-dimensional plane cutting through a three-dimensional body[12]

$$\sum N_i + \frac{1}{2}\sum N_i' - \sum S_i - \frac{1}{2}\sum S_i' = -1$$

Note that an alternate topological form was presented by Su et al.[17] in which S_5' would be replaced by a half-node N_3' and two half-saddles S_5' and S_6' symmetric about N_3'. This form, although satisfying the earlier topological rule, does not necessarily influence the topology of the flow on the lee side of the wing.

It should be noted that secondary and/or tertiary vortices are often observed underneath the primary vortex, especially at low angles of attack and smaller values of sweep angle. Their presence does not disturb the topological balance as they provide a self-balanced set of saddle and nodal points. These secondary and/or tertiary features are omitted from the typical topology in Fig. 10, as well as in Figs. 7 and 9, since they do not appear in the present data.

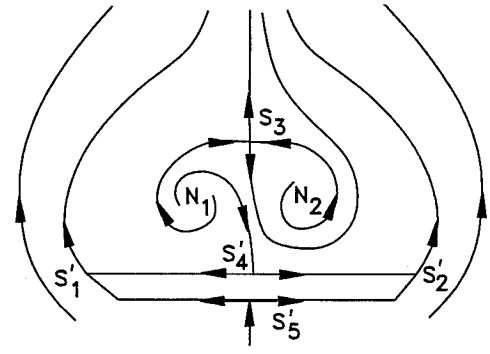

Fig. 9 Definition of topology of instantaneous streamline pattern at $\xi = 0.79$ and $\alpha = 45$ deg during pitch-up motion from $\alpha_i = 25$ deg to $\alpha_f = 50$ deg with various pitch rates from $\hat{A} = 0.025$ to 0.15. Pattern shown is in moving reference frame.

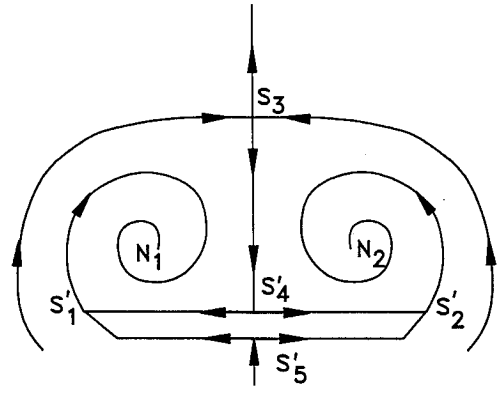

Fig. 10 Definition of topology of flow over delta wing at stationary, low angle of attack ($\alpha = 20$ deg). Definition constructed from data of Magness et al.,[3] Carcaillet et al.,[16] and Su et al.[17]

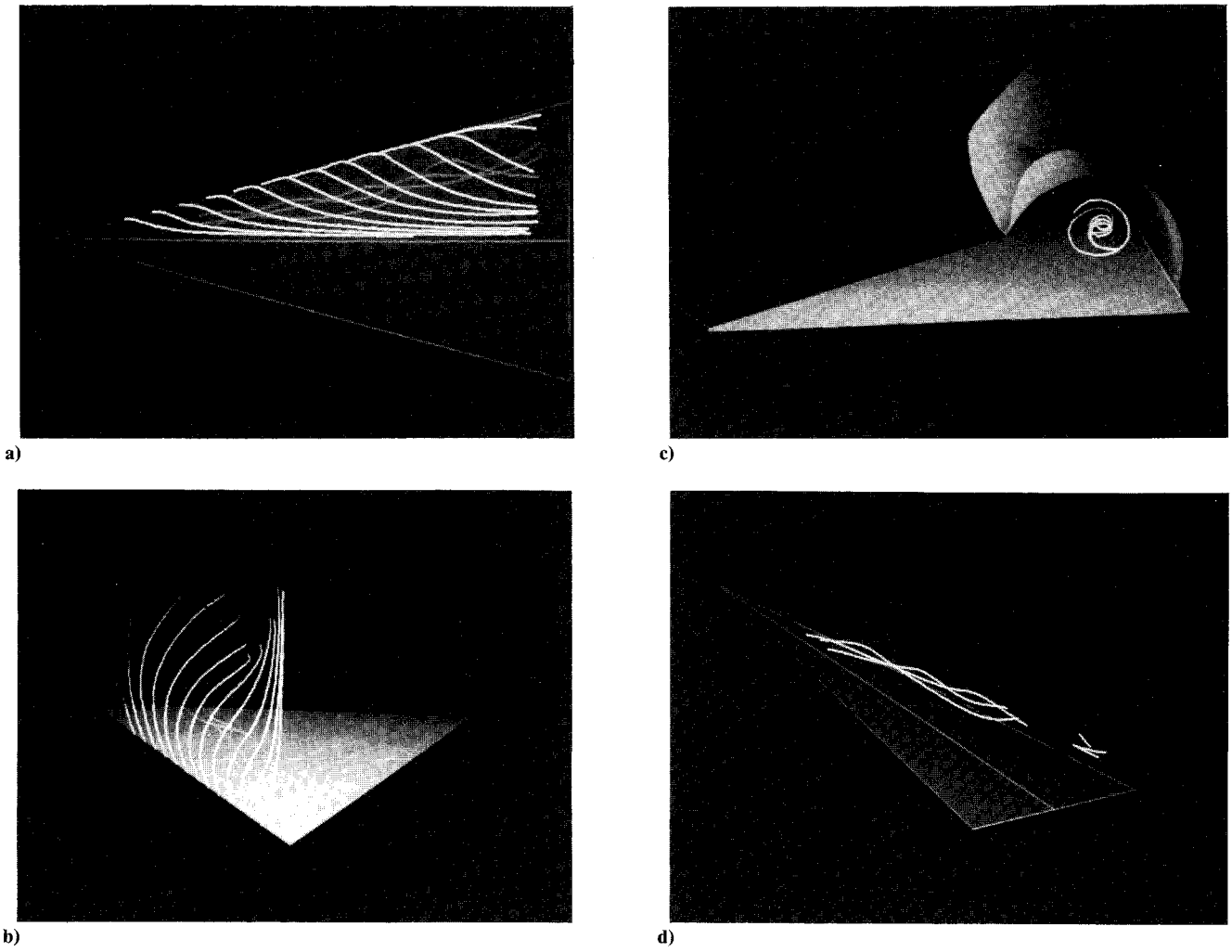

Fig. 11 Three-dimensional streamlines over pitching delta wing constructed from phase-locked data at α = 45 deg during pitch-up maneuver from α_i = 25 deg to α_f = 50 deg with pitch rate Å = 0.15. Views correspond to a) plan view of delta wing, b) downstream-looking view of delta wing, c) end view of leading-edge vortex, d) oblique view of delta wing. In a) and b) all streamlines are shown as lines. In c) and d) streamlines emanating from leading-edge are shown as solid surfaces; streamlines in "core" of vortex shown as lines.

The most important difference between Fig. 7 and Fig. 10 is that the two foci N_1 and N_2 are unstable (outward spiraling) in Fig. 7, whereas they are stable (inward spiraling) in Fig. 10. The inward spiral is the conventional interpretation of the leading-edge vortex. This major topological alteration during motion of the wing at high angle of attack results in a significant change in the mass flux properties of the vortex field, especially with regard to the flow into the region defined by the saddle point S_3.

In all of the cases noted herein, the centerline saddle points (S_3 in each figure) are all canonical in form. That is, their axes are orthogonal, which indicates that the flow there is irrotational in nature. Therefore, the vorticity in the leading-edge vortex, whether stable or unstable, is essentially concentrated in the core region. Moreover, under inviscid conditions, these points represent pressure maxima.[13]

Three-Dimensional Construction of the Leading-Edge Vortex

The three-dimensional velocity field and streamline pattern may be constructed from planes of two-dimensional data by integration of the continuity equation. Details of the construction technique are given by Robinson and Rockwell.[31] Its application for the present flow is addressed by Magness.[22] Twenty chordwise planes of two-dimensional data are first acquired during separate, phase-referenced realizations of the pitching motion. The repeatability of the phase-referencing scheme was established by comparing the interrogated velocity fields from multiple realizations of the same flow and pitching conditions. That is, multiple photographs were taken under identical conditions and processed. The basic features of the flow and the topological structure were found not to deviate from realization to realization. This result, as well as the configuration of these planes with respect to the delta wing, may be found in Magness.[22] The nondimensional spacing between planes was $\Delta\xi$ = 0.054. These planes of data are interpolated independently in regions where data dropout is present. A spectral technique is used to integrate the continuity equation along lines connecting the corresponding data locations in each plane. Planes of data are acquired sufficiently far upstream of the wing to approximate the freestream condition. Because of the relatively large sweep angle of the wing, the apex region induced little flow distortion and the freestream condition is satisfied at a nondimensional location of ξ = −0.108. At the ξ = −0.108 plane, the third velocity component is calculated from the known value of the freestream velocity. This plane provides the starting condition for the integration.

Figures 11a and 11b present two views of the instantaneous streamlines corresponding to a pitch-up motion at a pitch rate of Å = 0.15. Streamline patterns both within the vortex core and from the leading edge are illustrated therein. Figures 11c and 11d show the streamlines separating from the leading edge as a solid stream surface.

A striking feature of these photos is that there is no obvious sign of vortex breakdown; that is, there is no sudden radial expansion of the core streamline pattern or onset of turbulent motion, although the instantaneous angle of attack of the wing is 45 deg. The corresponding breakdown location for the stationary wing is nominally at ξ = 0.25. This difference in breakdown locations, addressed by Magness et al.[3] and Magness,[22] is because the response time scale for vortex breakdown is much larger than the convective time scale C/U_∞.

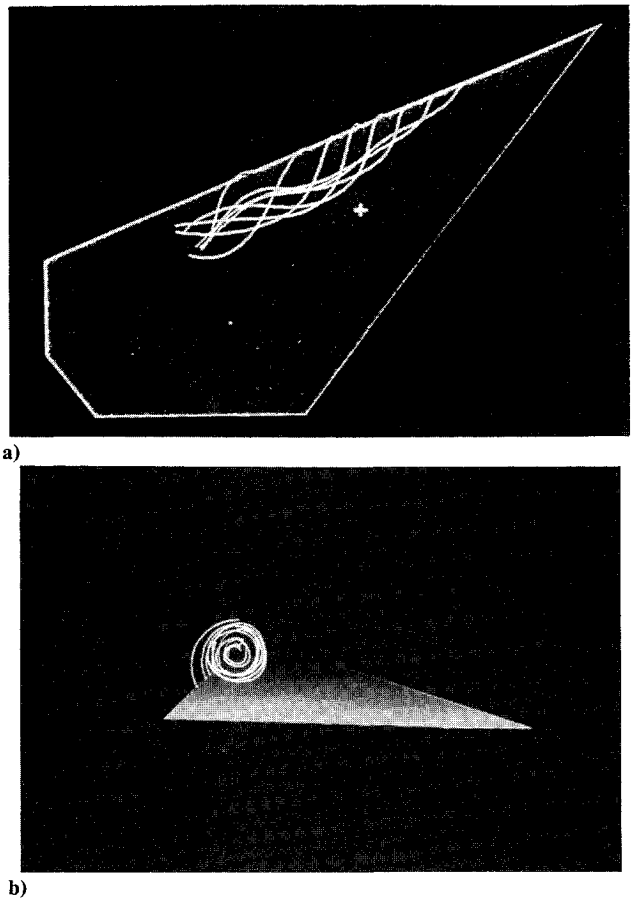

Fig. 12 Three-dimensional streamlines over stationary delta wing constructed from data at α = 20 deg (Magness et al.[3]). All streamlines shown as lines. Views correspond to a) plan view of delta wing and b) end view of leading-edge vortex.

Comparison of Fig. 12, corresponding to a stationary wing at α = 20 deg (Magness et al.[3]), with the pitching wing of Fig. 11 (α = 45 deg, pitch up) shows a difference in the three-dimensional streamline patterns consistent with the difference in the cross-sectional topology given in Figs. 9 and 10. For the case at α = 20 deg, the leading-edge vortex spirals inward along the entire leading edge. For α = 45 deg during the pitch-up motion, only the central portion of the vortex exhibits a spiral form; the outer streamlines originating from the leading edge tend to form a sheath over the vortex core and are swept downstream along the centerline of the wing before they complete one spiral revolution. This effect is particularly evident in Figs. 11c and 11d in which the separating stream surface is shown from two different perspectives. Upstream, close to the apex of the wing, the separating flow has a tendency to follow the freestream as in a bluff body wake. As the vortex develops downstream, however, the separating flow is drawn partially around the vortex core before it escapes into the wake. In the end view of Fig. 11c, the vortex is seen to exhibit the outward spiraling noted in the sectional streamline patterns of Fig. 6.

IV. Concluding Remarks

During pitch up of the delta wing to angles of incidence above the critical angle of attack, a change in topology is noted. In the aft region above the wing, the leading-edge vortex appears as an unstable focus. As a result of this major change in the nature of the leading-edge vortex, the entire crossflow topology undergoes a dramatic alteration. This alteration of the topology is observed for a variety of pitching rates from Å = 0.025 to 0.15 over a major portion of the wing.

Perry and Steiner[2] have shown the existence of an unstable focus in the wake of a two-dimensional flat plate at large incidence to the freestream. This structure is only possible in three-dimensional or marginally three-dimensional flows. This three-dimensionality allows for mass transport near the center of the focus to preserve continuity. Furthermore, the unstable focus represents an axially-compressed vortex filament,[33] which is the converse of the axially stretched filament present in a stable focus. Consequently, the unstable focus suggests an axial deceleration; the converse of this, namely, axial acceleration in the form of stable foci, is noted in propeller wake vortices.[33] For the present case, we can conclude that a substantial chordwise extent of the vortex core is undergoing compression. It may be hypothesized that the rapid, transient pitch-up motion of the wing enhances compression of the core vortex filament and induces an unstable focus.

The three-dimensional flowfield is constructed at an instant during the pitch-up motion at which the unstable focus is observed. Quite clearly, there is a coherent vortical flow structure over the entire wing at an instantaneous angle of attack of α = 45 deg, in contrast to the incoherent flow found over a large portion of the stationary wing at high angle of attack. There is, however, an instantaneous lack of entrainment of flow from the freestream as depicted by the instantaneous separation surface from the leading edge. The separation surface exhibits insignificant inward spiraling as normally occurs on the stationary wing at low angle of attack. This behavior is apparent over about the latter 80% of the wing chord. The core flow, however, does exhibit spiraling of the outward sense in addition to a significant streamwise flow component over the entire chord of the wing.

The instantaneous lack of entrainment of flow from the freestream into the core of the vortex should not be significantly influenced by the laminar or turbulent state of the shear layer. The shear layer in the present case is laminar; turbulent cases were not investigated. However, it appears that the large-amplitude motion imposed on the wing dominates the instantaneous distortion of this feeding sheet and overshadows any local effects due to the state of the separating shear layer.

The region adjacent to the leading edge of the wing, located between the feeding sheet and the outward spiraling vortex, does not exhibit a vortex pattern, evident by considering the instantaneous velocity field in Fig. 4. Based on these data, as well as other representations of the velocity field in the form of raw, unbiased images, this region appears to exhibit localized stall, in contrast to the secondary/tertiary vortices present on the stationary wing at low angle of attack.

Because of the limited resolution of the data in the immediate vicinity of the vortex core at stations near the wing apex, it is not possible to definitively state that the structure of the leading-edge vortex transforms from a stable to an unstable focus. If there were not such a transformation, however, the question is raised as to how the vorticity would be conducted into the vortex core and thereafter convected to downstream locations. A transformation along a vortex line similar to that discussed by Dallman[11] is an interesting prospect. Such a transition may require a point of symmetry in the strain field or, at a minimum, a plane of zero strain. In the present flow, one may envision a crossflow plane of zero strain due to the superposition of the natural straining with the destabilizing effect of the pitching motion. At that plane, the vortex would undergo transition from a stable to an unstable focus. Moreover, changes in angle of attack will alter the balance of strain, thus moving the plane of transformation. Changes in the pitch rate would induce similar effects. Thus, the transition should propagate along the chord of the wing.

Resolution of this matter poses several key questions, most importantly the extent and parametrical domain of the unstable focus. Furthermore, correlation of this observed behavior with force and moment measurements requires a detailed examination of the chordwise variation of the circulation of the leading-edge vortex for both stable and unstable modes, as well as its structure. Complicating these issues are the differing regimes of flow structure encountered at various angles of attack; especially those in the presence of vortex breakdown. These unresolved questions necessitate further investigation of this class of flows.

Acknowledgment

The authors appreciate the support of the Air Force Office of Scientific Research.

References

[1]Ashley, H., "On the Feasibility of Low-Speed Aircraft Maneuvers Involving Extreme Angles of Attack," *Journal of Fluids and Structures,* Vol. 1, 1987, pp. 319–335.

[2]Reynolds, G., and Abtahi, A. A., "Instabilities in Leading-Edge Vortex Development," AIAA Paper 87-2424, 1987.

[3]Magness, C., Robinson, O., and Rockwell, D., "Control of Leading-Edge Vortices on a Delta Wing," AIAA Paper 89-0999, 1989.

[4]Jarrah, M. A. M., "Visualization of the Flow about a Delta Wing Maneuvering in Pitch to Very High Angle of Attack," *International Symposium on Nonsteady Fluid Dynamics,* edited by J. A. Miller and D. P. Telionis, American Society of Mechanical Engineers, ASME Fluids Engineering Div., New York, 1990, pp. 109–116.

[5]Atta, R., and Rockwell, D., "Hysteresis of Vortex Development and Breakdown on an Oscillating Delta Wing," *AIAA Journal,* Vol. 25, No. 11, 1987, pp. 1512–1513.

[6]LeMay, S. P., Batill, S. M., and Nelson, R. C., "Vortex Dynamics on a Pitching Delta Wing," *Journal of Aircraft,* Vol. 27, No. 2, 1990, pp. 131–138.

[7]Woffelt, K. W., "Investigation of the Movement of Vortex Burst Position with Dynamically Changing Angle of Attack for a Schematic Delta Wing in a Water Tunnel with Correlation to Similar Studies in Wind Tunnels," *Aerodynamic and Related Hydrodynamic Studies Using Water Facilities,* AGARD CP-413, 1986.

[8]Soltani M. R., Bragg, M. B., and Brandon, J. M., "Measurements on an Oscillating 70-Deg Delta Wing in Subsonic Flow," *Journal of Aircraft,* Vol. 27, No. 3, 1990, pp. 211–217.

[9]Ashley, H., Katz, J., Jarrah, M. A. M., and Vaneck, T., "Unsteady Aerodynamic Loading of Delta Wings for Low and High Angles of Attack," *International Symposium on Nonsteady Fluid Dynamics,* edited by J. A. Miller and D. P. Telionis, Vol. 92, American Society of Mechanical Engineers, ASME Fluids Engineering Div., New York, 1990, pp. 61–78.

[10]Magness, C., Robinson O., and Rockwell D., "Unsteady Delta Wing Crossflow Using Particle Image Velocimetry," *Journal of Aircraft*, Vol. 29, No. 4, 1992, pp. 707–709.

[11]Dallman, U., "Structural Stability of Three-Dimensional Vortex Flows," *Nonlinear Dynamics in Transcritical Flows,* edited by H. L. Jordan, H. Oertel, and K. Robert, Springer-Verlag, Berlin, Germany,1985.

[12]Hunt, J. C. R., Abell, C. J., Peterka, J. A., and Woo, H., "Kinematical Studies of the Flows Around Free or Surface-Mounted Obstacles; Applying Topology to Flow Visualization," *Journal of Fluid Mechanics,* Vol. 86, 1978, pp. 179–200.

[13]Hornung, H., and Perry, A. E., "Some Aspects of Three-Dimensional Separation, Part 1: Streamsurface Bifurcations," *Zeitschrift für Flugwissenschaften und Weltraumforschung*, Vol, 8, 1984, pp. 77–87.

[14]Chong, M. S., Perry, A. E., and Cantwell, B. J., "A General Classification of Three-Dimensional Flow Fields," *Physics of Fluids A,* Vol. 2, 1990, pp. 765–777.

[15]Tobak, M., and Peake, D. J., "Topology of Three-Dimensional Separated Flows," *Annual Review of Fluid Mechanics,* Vol. 14, 1982, pp. 61–85.

[16]Carcaillet, R., Manie, F., Pagan, D., and Solignac, J. L., "Leading Edge Vortex Flow Over a 75 Degree Swept Delta Wing: Experimental and Computational Results," *Proceedings of the 15th ICAS Conference,* London, Sept. 1986.

[17]Su, W., Liu, M., and Liu, Z., "Topological Structures of Separated Flows About a Series of Sharp-Edged Delta Wings at Angles of Attack up to 90°," *Topological Fluid Mechanics,* edited by H. K. Moffatt and A. Tsinober, Cambridge, 1990, pp. 395–407.

[18]Magness, C., Robinson, O., and Rockwell, D., "Flow Structure on a Pitching Delta Wing," *Bulletin of the American Physical Society,* Abstract KE-5, Vol. 35, 1990, p. 2335.

[19]Dudderar, T. D., Meynart, R., and Simpkins, P.G., "Full-Field Laser Metrology for Fluid Velocity Measurement," *Optics and Lasers in Engineering,* Vol. 9, 1988, pp. 163–199.

[20]Adrian, R. J., "Particle-Imaging Techniques for Experimental Fluid Mechanics," *Annual Review of Fluid Mechanics,* Vol. 23, 1991, pp. 261–304.

[21]Magness, C., Robinson, O., and Rockwell, D., "Laser Scanning Particle Image Velocimetry Applied to a Delta Wing in Transient Maneuver," *Experiments in Fluids* (to be published).

[22]Magness, C., "Unsteady Response of Leading-Edge Vortices on a Pitching Delta Wing," Ph.D. Dissertation, Dept. of Mechanical Engineering and Mechanics, Lehigh Univ., Bethlehem, PA, 1991.

[23]Lourenco, L., and Krothapalli, A., "The Role of Photographic Parameters in Laser Speckle or Particle Image Displacement Velocimetry," *Experiments in Fluids,* Vol. 5, 1987, pp. 29–32.

[24]Adrian, R. J., "An Image Shifting Technique to Resolve Directional Ambiguity in Double-Pulsed Laser Velocimetry," *Applied Optics,* Vol. 25, 1986, pp. 3855–3858.

[25]Meynart, R., "Instantaneous Velocity Field Measurements in Unsteady Gas Flow by Speckle Velocimetry," *Applied Optics,* Vol. 22, 1983, pp. 535–540.

[26]Lourenco, L. and Krothapalli, A., "Particle Image Displacement Velocimetry Measurements of a Three-Dimensional Jet," *Physics of Fluids,* Vol. 31, 1988, pp. 1835–1837.

[27]Lourenco, L., Krothapalli, A., Buchlin, J. M., and Riethmuller, M. L., "A Non-Invasive Experimental Technique for the Measurement of Unsteady Velocity and Vorticity Fields," *Aerodynamic and Related Hydrodynamic Studies Using Water Facilities,* AGARD CP-413, 1986.

[28]Landreth, C. C., and Adrian, R. J., "Measurement and Refinement of Velocity Data Using High Image Density Analysis in Particle Image Velocimetry," *Applications of Laser Anemometry to Fluid Mechanics: Proceedings of the 4th International Symposium,* edited by R. J. Adrian, Springer-Verlag, New York, 1989, pp. 484–497.

[29]Perry, A. E., and Chong, M. S., "A Description of Eddying Motions and Flow Patterns Using Critical-Point Concepts," *Annual Review of Fluid Mechanics,* Vol. 19, 1987, pp. 125–155.

[30]Payne, F. M., and Nelson, R. C., "An Experimental Investigation of Vortex Breakdown on a Delta Wing," *Vortex Flow Aerodynamics*, edited by J. F. Campbell, R. F. Osborn, and J. T. Foughner, NASA CP-2416, 1986, pp. 135–161.

[31]Robinson, O., and Rockwell, D., "Construction of Three-Dimensional Images of Flow Structure via Particle Tracking Techniques," *Experiments in Fluids,* Vol. 14, 1993, pp. 257–270.

[32]Perry, A. E., and Steiner, T. R., "Large-Scale Vortex Structures in Turbulent Wakes Behind Bluff Bodies; Part 1: Vortex Formation," *Journal of Fluid Mechanics,* Vol. 174, 1987, pp. 233–270.

[33]Perry, A. E., and Steiner, T. R., "Large-Scale Vortex Structures in Turbulent Wakes Behind Bluff Bodies; Part 2: Far-Wake Structures," *Journal of Fluid Mechanics,* Vol. 174, 1987, pp. 271–298.